Fermi National Accelerator Laboratory

FERMILAB-TM-2047

Electron Beam Distortions in Beam-Beam Compensation Set-Up

Vladimir Shiltsev and Alexander Zinchenko

Fermi National Accelerator Laboratory
P.O. Box 500, Batavia, Illinois 60510

April 1998

Operated by Universities Research Association Inc. under Contract No. DE-AC02-76CH03000 with the United States Department of Energy

Disclaimer

Distribution

Electron Beam Distortions in Beam-Beam Compensation Set-Up

Vladimir Shiltsev and Alexander Zinchenko*
Fermi National Accelerator Laboratory, Batavia, IL 60510, USA
(April 30, 1998)

This article is devoted to electron beam distortions in the "electron compressor" setup for beam-beam compensation in the Tevatron collider. Effects of electron space charge force and interaction of the electron beam with impacting elliptical antiproton beam are studied. We make an estimate of longitudinal magnetic field necessary to keep the electron beam distortions low.

41.20.-q, 41.75.Fr, 41.85.Ct, 29.27.Fh

I. INTRODUCTION

An idea of compensation of beam-beam effects in the Tevatron collider with use of high current, low energy electron beam was presented in Refs. [1], [2]. Modifications of the proposal are 1) the "electron lens" with modulated current which is supposed to provide different linear defocusing forces for different antiproton bunches (spaced by τ=132 ns in the Tevatron'33 upgrade project [3]) and, therefore, equalize their betatron frequencies which are not naturally equal due to proton-antiproton interaction in numerous parasitic crossings along the ring; and 2) the "electron compressor", essentially nonlinear but DC electron lens to compensate (in average) the non-linear focusing of antiprotons due to proton beam and, thus, to reduce the beam-beam footprint. The electron beam setup looks much like an electron cooler, except electrons collide with antiprotons (proton beam is separated from the latter two). About 2-m long, 2-mm diameter, 10 kV electron beam with 1-2 Amperes of current is to be installed in a place with large beta-function($\sim$100m), away from the main interaction points (IPs - B0 and D0 at the Tevatron). A strong longitudinal magnetic field plays a significant role in maintaining stability of both electron and antiproton beams as well as in keeping the electron beam current distribution distortions and, therefore, distortions of electron space charge forces, within acceptable limits.

This article is focused mostly on the time-dependent deviations of the electron beam shape during passage of the interaction region. Consideration of other important effects, like a "head-tail" instability caused by wide band impedance due to electron beam, can be found elsewhere (see talks by Danilov, Burov and Shiltsev in [4]).

In Section 2 of this article we discuss results of numerical tracing of electron trajectories in the "electron compressor". Theoretical analysis of the distortions in drift approximation is presented in Section 3. Section 4 briefly summarizes our studies.

II. NUMERICAL TRACING OF ELECTRONS.

ZBEAM code [5] is used for tracing electron trajectories. This is essentially two dimensional code which takes into account only transverse components of the electric and magnetic forces. It is a good approximation for the forces due to ultra-relativistic $\bar{p}$ bunch and the electron space charge forces, as the electron beam to be either DC or to be comparatively slowly modulated with the spatial modulation scale of $\tau \cdot c \approx$ 40m much larger than transverse beam size of few mm.

The code solves an equation of motion of a charge. In the laboratory frame, in presence of some external electric and magnetic fields and in the presence of some additional moving electric charges, the equation is as follows:

$$m\frac{d^2\vec{r}}{dt^2} = q(\vec{E} + [\vec{v}\times\vec{B}] + \sum_{i=1}^{n}\vec{E}_i + \sum_{i=1}^{n}[\vec{v}\times\vec{B}_i]), \tag{1}$$

Here m, q and $\vec{v}$ are the particle mass, electric charge and velocity, $\vec{E}$ and $\vec{B}$ are external electric and magnetic fields, $\vec{E}_i$ and $\vec{B}_i$ are the electric and magnetic fields of a bunch "macroparticle":

$$\vec{E}_i = \frac{q_i(Z)\vec{r}}{2\pi\epsilon_0 r^2}, \qquad \vec{B}_i = \frac{1}{c^2}[\vec{v}_i\times\vec{E}_i]. \tag{2}$$

Tracking of a particle is achieved by integrating the equation of motion over successive small time steps.

Fig.1 shows trajectories vs. longitudinal coordinate z for electrons which originally had no transverse velocities and started at radii equal to r_0 =0.1, 0.5, 0.8 and 0.9 mm in absence of longitudinal magnetic field. Left plot demonstrates disruption under impact of the self space charge forces in round electron beam with constant transverse current distribution with following parameters: the beam radius $a = 0.9$ mm, total current $J_e = 1.5$A, kinetic energy of electrons $U_e = 10$ kV. One can see many fold increase of the beam size over 180 cm long path. Note, that the electron trajectories do not intersect each other, therefore, the particle at the border $r_0 = 0.9$mm always stays at the border.

Right plot in Fig.1 shows trajectories of the same particles under impact of oncoming bunch of $N_{\bar{p}} = 6 \cdot 10^{10}$ antiprotons having Gaussian distributions with rms radial size of $\sigma_r = 0.9$mm and longitudinal rms size of $\sigma_z = 30$cm, and the electron space-charge is off. Again, significant electron beam size increase is seen, nevertheless, it is somewhat less than at the left plot (final radius of about 50 mm instead of 120 mm). Note, that 1800 mm path corresponds to the time for all antiprotons within $\pm 3 \cdot \sigma_z$ to add their impact to the electrons' motion. Now the trajectories intersect each other, thus, the particle originally being at the border of the electron beam, got the least angular deflection.

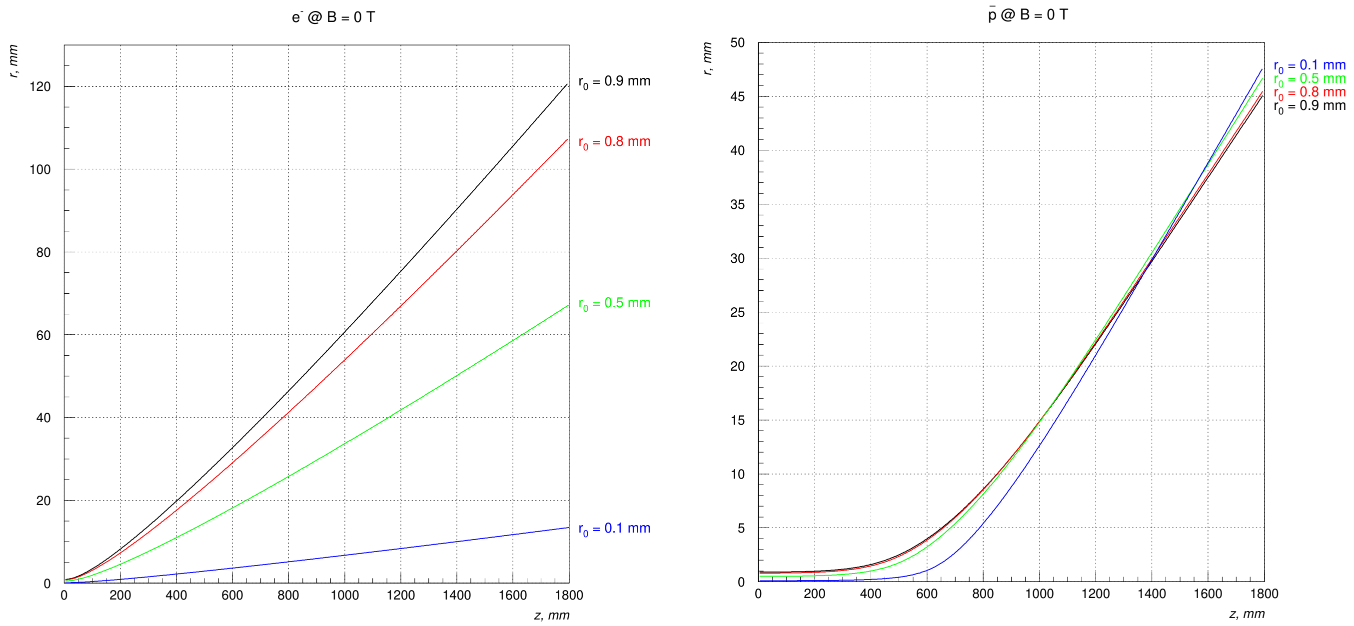

FIG. 1. Expansion of the electron beam due to self-field (left) and trajectories of electrons inside $\bar{p}$-bunch (right).

Solenoid magnetic field in the set-up for the beam-beam compensation allows to avoid the disruption of high current electron beam. It was shown in Ref. [1], that stability of the electron beam in a solenoidal field B requires its focusing strength to be more than defocusing due to electron and antiproton space-charge defocusing:

$$\frac{1}{F_B^2} \geq \frac{1}{F_e^2} + \frac{1}{F_{\bar{p}}^2}, \tag{3}$$

where the effective focal length due to the magnetic field B is

$$F_B = \frac{2\gamma_e \beta_e m_e c^2}{eB} \approx 3.3[cm]\frac{\gamma_e \beta_e}{B[kG]}, \tag{4}$$

here $\beta_e = v_e/c = \sqrt{2U_e/mc^2}$ and $\gamma_e = 1/\sqrt{(1-\beta_e^2)}$ are relativistic factors. E.g., for 10 kV electrons $\beta_e = 0.2$ and

$$F_B = 0.66[cm]/B[kG].$$

The defocusing length due to electron space charge of the 1.5 A 10 kV electron beam is

$$F_e = \sqrt{\frac{J_0 \gamma_e^3 \beta_e^3 a_e^2}{2J_e}} \approx 0.77[cm], \quad J_0 = mc^3/e = 17\ kA. \tag{5}$$

The minimum defocusing length due to the pbar beam is

$$F_{\bar{p}} = \sqrt{\frac{\gamma_e \beta_e^2 \sqrt{2\pi} \sigma_z \sigma_r^2 m_e c^2}{e^2 N_{\bar{p}} (1+\beta_e)}} \approx 1.11[cm], \tag{6}$$

where we take the same parameters as above – $N_{\bar{p}} = 6 \cdot 10^{10}$, $\sigma_r = 0.9$ mm, $\sigma_z = 30$cm.

The electron beam is stable if the focusing term $1/F_B^2$ in Eq.(3) is stronger than the two defocusing terms, that corresponds to $B \geq 1\,kG$ for non-relativistic electrons. Note, that the electron space charge defocusing is about 1.5 times the one due to pbar beam forces, therefore, an approximate scaling law is valid for minimum stabilizing solenoid field:

$$B_{min} \propto \frac{J_e^{1/2}}{a_e},\ a_e \simeq \sigma_r. \tag{7}$$

For example, doubling the electron current requires only $\sqrt{2} \approx 1.41$ more magnetic field strength.

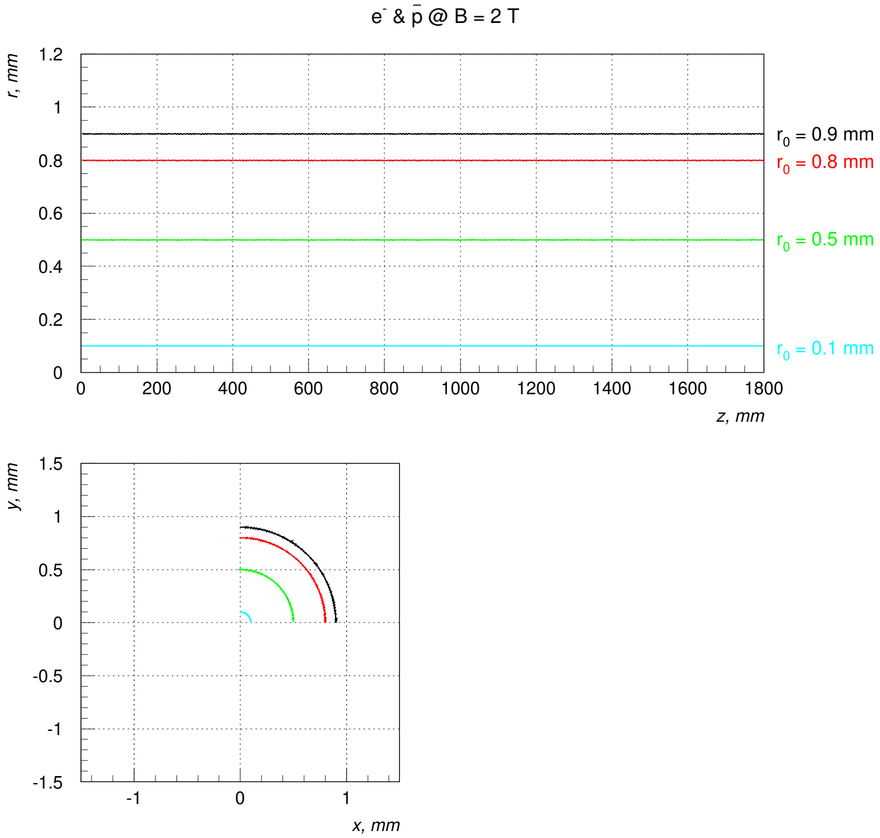

FIG. 2. Electron beam behavior inside $\bar{p}$ bunch at 2 T.

Fig.2 presents electron trajectories in B =2T solenoidal magnet with taking into account impact of both electron and antiproton space charge forces. The electrons are assumed to be brought to the interaction region adiabatically, i.e. without excitation of their transverse Larmor oscillations with spatial period of $\lambda_L = v_e/\omega_L = \beta_e mc^2/eB \approx 3.4[mm]/B[kG]$. The $\bar{p}$ bunch length is much longer than λ_L, and, therefore, antiprotons repulse electrons adiabatically and do not excite the Larmor oscillations – one can see no radius variations in the top plot of Fig.2.

The only effect of the space charge forces is an azimuthal drift of electrons as it is presented in the lower plot of Fig.2. One can see that all electron trajectories started having Y coordinate equal to 0, but during the passage time all the particles have been rotated while staying on the same radii. The drift velocity in crossed electric and magnetic fields $\vec{E}$ and $\vec{B}$ is equal to:

$$\vec{v}_d = c\frac{[\vec{E} \times \vec{B}]}{B^2}. \tag{8}$$

The space charge electric field inside constant current density $j = J_e/\pi a_e^2$ is proportional to radius $\vec{E} = 2j\vec{r}/\beta_e$, and, therefore, the angle θ_d of the drift rotation over the time interval t does not depend on radius $\theta_d = v_d t/r = 2jct/\beta_e B$. The electric field due to Gaussian $\bar{p}$ beam is not linear, that concludes that the rotation angle θ_d is no longer independent of r, and electrons with larger r perform drift rotation on different (smaller) angle, although the difference is negligible under parameters we used - see lower plot in Fig.2. [1]

One can conclude that the interaction with round $\bar{p}$ bunch in strong magnetic field conserves axial symmetry and radial size of the electron beam, and, therefore, the electron beam space charge forces are the same for antiprotons at the head and at the tail of the $\bar{p}$ bunch. It is no longer true if electron or antiproton beam is not round. Roundness of the electron beam can be assured by using round cathode in the electron gun and by appropriate choice of the magnetic field in the transport section of the set-up. In opposite, the $\bar{p}$ beam roundness can be achieved in very few Tevatron locations where vertical and horizontal beta-functions are the same $\beta_x = \beta_y$ (vertical and horizontal emittances of 1000 GeV beams in the Tevatron are approximately equal $\varepsilon_{x,y}^{rms} \approx 3.3\pi\, mm \cdot mrad$). *A priori* this condition can not be fulfilled. E.g., at present stage we consider to install one of the "electron lens" devices at the Tevatron F48 location which is characterized by $\beta_x = 101.7$ m and $\beta_y = 30.9$ m, and, consequently, the rms bunch sizes are $\sigma_x = 0.61$mm and $\sigma_y = 0.31$mm [2].

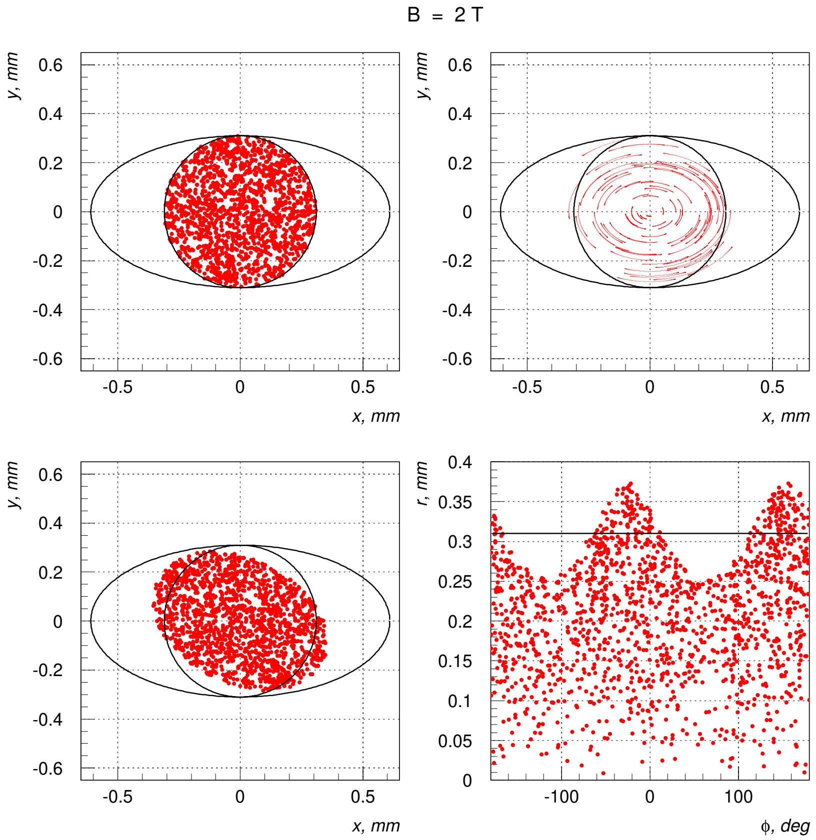

FIG. 3. "Small" electron beam distortion due to $\bar{p}$ bunch.

Fig.3 shows what happens with round electron beam (radius $a_e = 0.31$mm) while it interacts with such an antiproton beam being in 2T solenoid field. *ZBEAM* code is used for the electric field calculations and electron tracing. Top left plot shows an ellipse which corresponds to 1σ of the Gaussian $\bar{p}$ bunch and a circle of the electron beam cross section uniformly filled with electron macroparticles before the interaction with $\bar{p}$-s. Top right plot demonstrates traces of the electrons under impact of asymmetric electric field of the antiproton bunch. Resulted macroparticle positions and

[1]In fact, the magnetic forces produced by electron and antiproton currents produce additional drifts similar to electric ones, but their contributions are β_e^2 and β_e times smaller and, therefore, negligible. Nevertheless, it will be taken into account in the formulae of the Section 3.

the shape of the electron beam in $x-y$ and $r-\phi$ planes are shown in lower left and right plots of Fig.3 respectively. One can see that the electron beam becomes a rotated ellipse to the moment when the tail of antiproton bunch passes it through, while the head of the bunch sees originally undisturbed round electron beam. This might be of concern because of two reasons: 1) there appears a "head-tail" interaction in the $\bar{p}$ bunch via higher than dipole wake fields propagating in the electron beam; 2) in addition to useful defocusing effect, electric fields of the elliptic electron beam produce effective $x-y$ coupling of vertical and horizontal betatron oscillations in the $\bar{p}$ beam.

In the following section we analyze the effect and consider ways to reduce the distortion.

III. ANALYSIS OF ELLIPTIC DISTORTIONS.

A. Distortion of electron density.

We start with continuity equation for the electron charge density $\rho(x, y, z, t)$:

$$\frac{\partial \rho}{\partial t} + \mathrm{div}(\rho \vec{\mathrm{v}}) = 0, \tag{9}$$

where $\vec{v}(x, y, z, t)$ is the velocity of electrons. Since longitudinal component of the velocity is constant $v_z = \beta_e c$ and all longitudinal scales (like $\bar{p}$ bunch length σ_z or electron beam length) are much longer than transverse scale; then, one can neglect the term $\partial/\partial z(\rho v_z)$ in (9). In previous Section, we found that the major component of transverse electron motion is the drift with velocity $\vec{v}_d$ from Eq.(8), while fast Larmor motion is negligible, therefore, in the further analysis we consider $\vec{v} = \vec{v}_d$. Now, if we assume that unperturbed charge distribution is axially symmetric $\rho(t=0) = \rho_0(r)$ and that maximum density distortion is small $\rho = \rho_0 + \delta\rho$, $\delta\rho \ll \rho_0$, then in the highest order one gets from (9):

$$\frac{\partial \rho}{\partial t} + \vec{v}_d \cdot \vec{\bigtriangledown} \rho_0 + \rho \mathrm{div} \vec{v}_d = 0. \tag{10}$$

The third term is equal to zero because $\mathrm{div}\vec{\mathrm{v}}_{\mathrm{d}} = 0$. The gradient in the second term is $\vec{\bigtriangledown}\rho_0 = 2\vec{r}d^2\rho_0(r^2)/d(r^2)$, thus, we obtain:

$$\vec{v}_d \cdot \vec{\bigtriangledown} \rho_0 = \frac{2c}{B^2} \frac{d\rho_0(r^2)}{d(r^2)} [\vec{E} \times \vec{B}] \cdot \vec{r}. \tag{11}$$

The electric field of the round electron beam does not contribute to the product above as it is proportional to $\vec{r}$. Its contribution in our case can be omitted in further analysis as long as the electron charge density distortions are small with respect to $\rho_0(r)$. The major reason of the density change $\delta\rho$ is the antiproton beam space charge force. The electric field of the elliptic Gaussian relativistic $\bar{p}$ beam is given by :

$$\vec{E} = -eN_{\bar{p}} \cdot \lambda(z) \cdot \vec{\bigtriangledown} U, \tag{12}$$

where linear density of antiprotons is normalized as $\int \lambda(z) dz = 1$, and the two dimensional interaction potential $U(x, y)$ is [6]:

$$U(x,y) = \int_0^\infty dq \frac{1 - \mathrm{e}^{-\frac{x^2}{2\sigma_x^2(1+qR)} - \frac{y^2}{2\sigma_y^2(1+q/R)}}}{\sqrt{(1+qR)(1+q/R)}}, \quad R = \frac{\sigma_y}{\sigma_x}. \tag{13}$$

Therefore, after some mathematics we get:

$$\delta\rho(x, y, t = \frac{z}{(1+\beta_e)c}) = \Big(\int_{-\infty}^{z} \lambda(z')dz'\Big) \cdot \frac{2eN_{\bar{p}}}{B} \frac{d\rho_0(r^2)}{d(r^2)} \cdot \frac{xyI(x,y)(\sigma_x^2 - \sigma_y^2)}{\sigma_x^2 \sigma_y^2}, \tag{14}$$

where now z is the coordinate inside the $\bar{p}$ bunch [2] and

---

[2] i.e. $z = -\infty$ is for the bunch head and $\int_{-\infty}^{z} \lambda(z')dz'$ is proportional to the antiproton charge which passed through the given part of the electron beam.

$$I(x,y)=\int_0^\infty dq \frac{\mathrm{e}^{-\frac{x^2}{2\sigma_x^2(1+qR)}-\frac{y^2}{2\sigma_y^2(1+q/R)}}}{(1+qR)^{3/2}(1+q/R)^{3/2}}, \quad I(0,0)=\frac{2R}{(1+R)^2}. \tag{15}$$

Now we can see major features of the resulted distortion: a) it is absent in the case of round $\bar{p}$ beam when $\sigma_x=\sigma_y$; b) it performs two variations over azimuth $\delta\rho \propto xy \sim sin(2\theta)$; 3) it vanishes with the solenoid field B increase, or decrease of antiproton intensity $N_{\bar{p}}$; 4) most of the distortion takes place at the radial edge of the electron beam, and, since $d\rho_0(r^2)/d(r^2) \simeq \rho_0^{max}/a_e^2$, then wider electron beam gets smaller density distortions during the interaction. Finally, the scaling of the maximum distortion strength is:

$$\frac{\delta\rho^{max}}{\rho_0^{max}} \sim \frac{0.2eN_{\bar{p}}}{a_e^2 B} \approx \frac{0.6[N_{\bar{p}}/6\cdot 10^{10}]}{a_e^2[mm]B[kG]}, \tag{16}$$

and value of 0.2 comes from geometrical factor $\propto xy\cdot I(x,y)$. For example, the distortion is about 3% for 1 mm radius electron beam in $B=20$kG=2T solenoid field. Note, that as soon as the elliptic distortion appeared it starts drift rotation in the crossed fields of electron space charge and the solenoid field. For us it is important that during the passage of the $\bar{p}$ bunch, which is about $\pm 2\sigma_z/c = 2$ns, the rotation is small – for example, in $B=$2T the angle is about $\theta_d \approx 4j\sigma_z a_e/\beta_e B \approx 0.1$rad $\ll 1$ – thus, ignoring of the factor $\vec{v}_d \cdot \vec{\bigtriangledown}\delta\rho$ in Eq.(10) is justified.

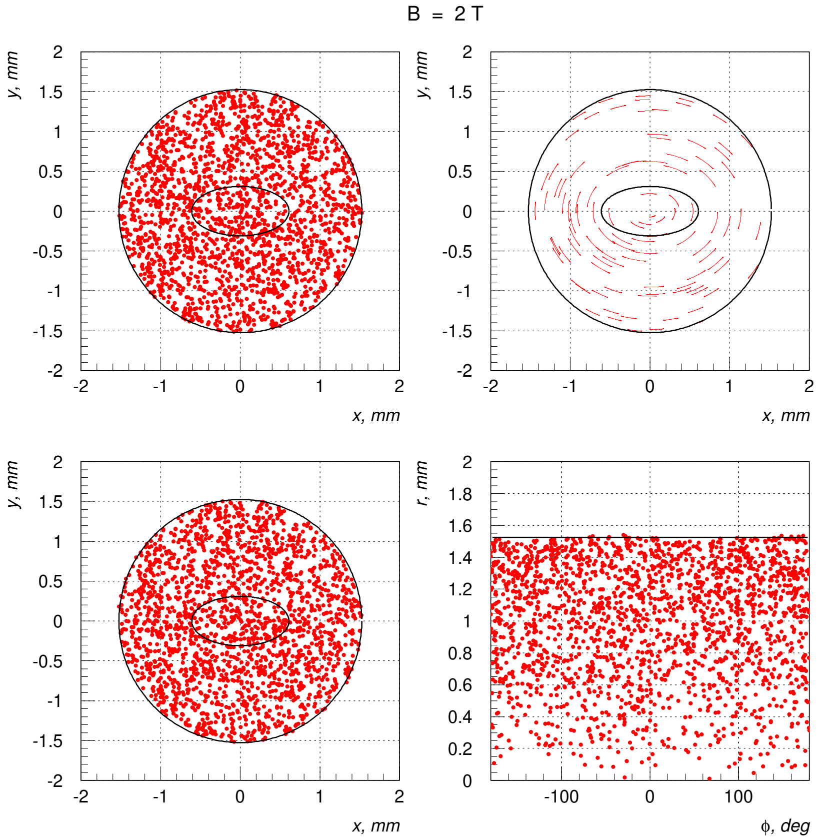

FIG. 4. Wide electron beam distortion due to narrow $\bar{p}$ bunch.

Fig.4 presents *ZBEAM* simulations of the constant density electron beam which is much wider than the $\bar{p}$ beam $a_e = 1.5$mm $\approx 2.5\sigma_x$. In opposite to the case presented in Fig.3, the electron beam distortions in the same field of $B=2$T are now very small $\simeq 2\%$.

Distortion of other than constant electron density can be calculated analytically with use of Eq.(14). For example, top left plot in Fig.5 shows lines of constant density for the electron beam with density of

$$\rho_0(r) = \frac{1}{1+(r/a_e)^{2\mu}}, \ \mu=3, \ a_e=\sigma_x=0.61\,\mathrm{mm}. \tag{17}$$

Here and below the x and y coordinates are given in units of σ_x.

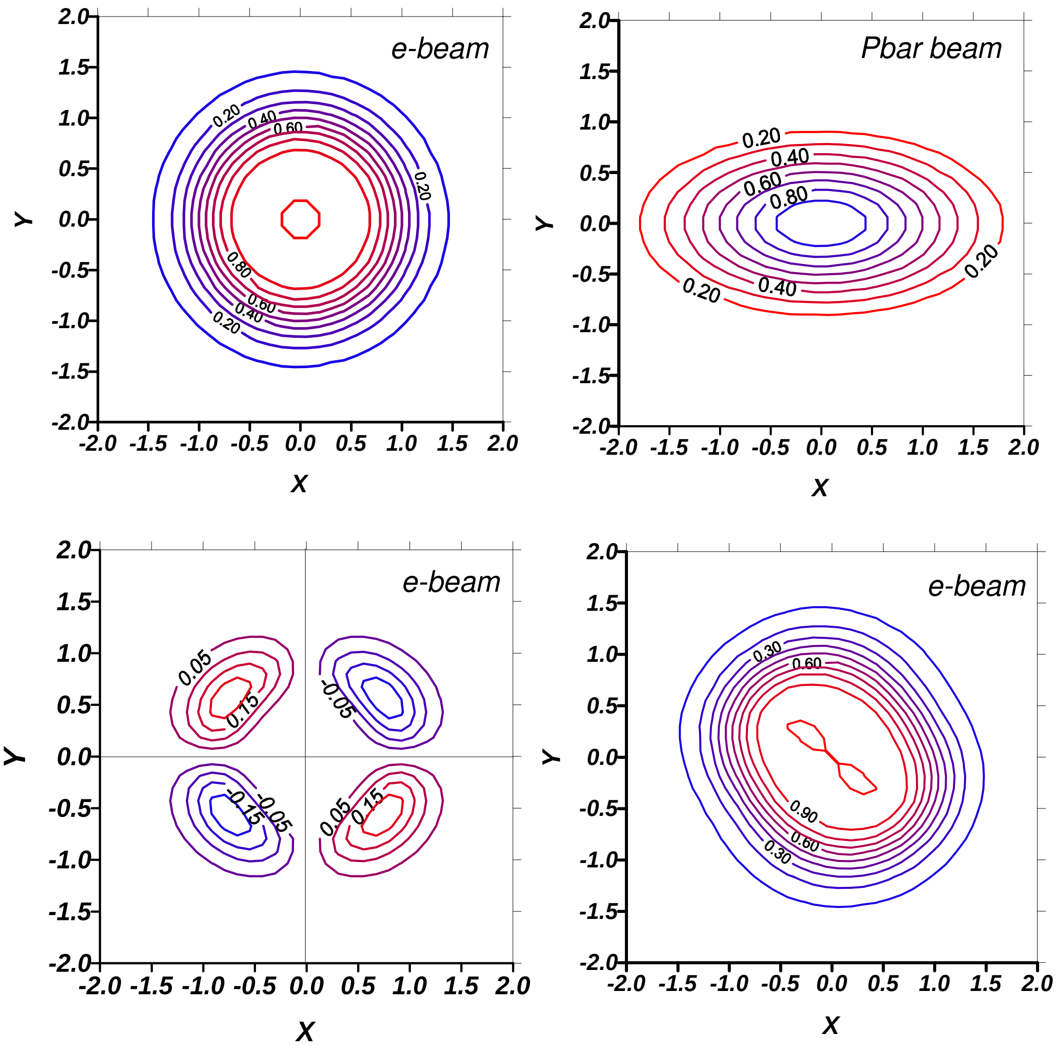

FIG. 5. Contour plots of original electron density (top left), $\bar{p}$ density (top right), change of the electron density due to interaction with $\bar{p}$ space charge (bottom left) and resulted electron density.

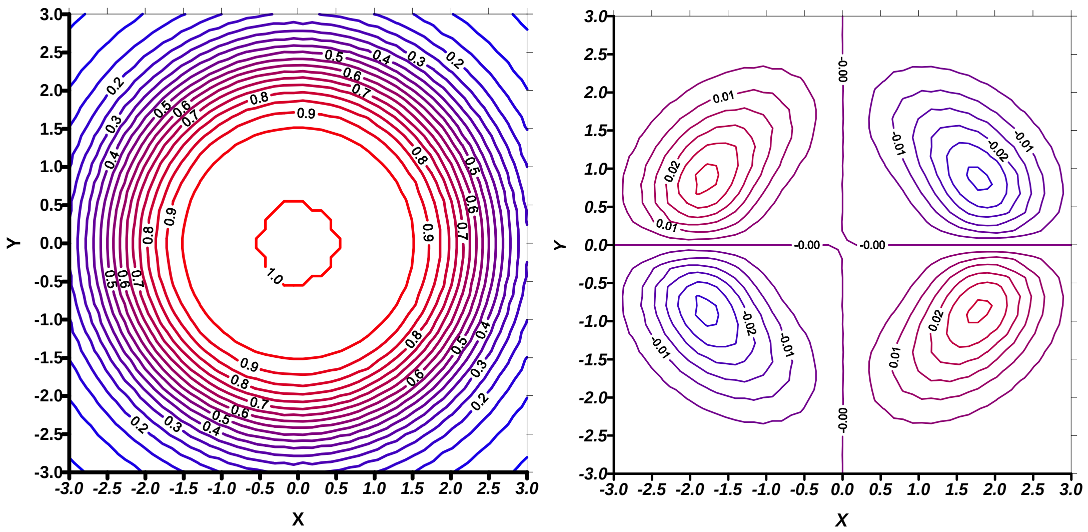

FIG. 6. Wider electron beam(left) and its distortion(right).

Constant density lines for the Gaussian distribution in the antiproton beam with $\sigma_x = 0.61$ mm and $\sigma_y = 0.31$mm are presented in the top right plot. Lower left corner of the Figure is for the change of the electron charge density $\delta\rho(x, y)$ after passage through the antiproton bunch with $N_{\bar{p}} = 6 \cdot 10^{10}$ in the magnetic field $B = 4$kG. With such small solenoid field the distortion is very large $\delta\rho^{max} \simeq 0.25$ and the resulted electron beam shape $\rho = \rho_0 + \delta\rho$ is now rotated ellipse as it is depicted in the lower right plot. Consequently, the space charge fields are very different for the antiprotons in the head and in the tail of the bunch.

After consideration of the Tevatron beam-beam tune footprint in presence of the "electron lens" in Ref. [2], there was found that an electron beam 2-3 times wider than the $\bar{p}$ beam size results in smaller footprint area. That also helps to reduce $\delta\rho$. Fig.6 demonstrates the electron beam distribution ρ_0 accordingly to Eq.(17) but with $a_e = 2.5\sigma_x = 1.5$mm – see left plot, and the resulted distortion $\delta\rho$ (right plot) which is now less than 0.05.

B. Coupling due to distorted electron beam.

Electric and magnetic fields of the elliptic electron beam lead to effective $x - y$ coupling of vertical and horizontal betatron oscillations in the $\bar{p}$ beam. Since originally the electron beam is round, the head of the $\bar{p}$ bunch experiences no coupling force. But, as the electron density distortion grows as $\int^z \lambda(z')dz'$, then the coupling grows proportionally. Particles in the head and in the tail of the bunch change their positions while performing synchrotron oscillations, thus, an average coupling effect is half of the maximum coupling spread. The average coupling can be corrected in the Tevatron, while there are no tools to compensate the spread in coupling. Therefore, the spread has to be small enough in order not to affect $\bar{p}$ beam dynamics.

The tunes of a small amplitude particle can be written as

$$\nu_\pm = \frac{\Big[(\nu_x + \Delta\nu_x) + (\nu_y + \Delta\nu_y)\Big]}{2} \pm \sqrt{\frac{\Big[(\nu_x + \Delta\nu_x) - (\nu_y + \Delta\nu_y)\Big]^2}{4} + |\kappa + \Delta\kappa|^2}, \tag{18}$$

where ν_x and ν_y are the unperturbed horizontal and vertical tunes (in the current Tevatron lattice they are 0.585 and 0.575 correspondingly), κ is a complex number describing the coupling (for satisfactory operation of the Tevatron collider, the global coupling is corrected down to value of $|\kappa| \approx 0.001$ [7]), and Δ's represent the changes of these quantities that arise from the interaction with the electron beam. The interaction is often described in terms of the two-dimensional potential $V(x, y)$, thus, the horizontal tune shift can be found from

$$\Delta\nu_x = -\frac{\beta_x}{4\pi}\frac{\partial^2 V}{\partial x^2}. \tag{19}$$

The coupling shift can be calculated as

$$\Delta\kappa = \frac{\sqrt{\beta_x\beta_y}e^{i(\psi_x - \psi_y)}}{4\pi}\frac{\partial^2 V}{\partial x \partial y}. \tag{20}$$

In the case of almost round electron beam with small elliptic distortion one can write $V(x, y) = V_0(r) + V_{skew}(xy)$. The potential V_0 and corresponding tune shift for round, constant density electron beam with total current J_e and total length L are equal to

$$V_0(r) = r^2\frac{(1 + \beta_e)J_e L r_{\bar{p}}}{e\beta_e c a_e^2 \gamma_{\bar{p}}},$$

$$\Delta\nu_x = -\frac{\beta_x}{4\pi}\frac{2(1 + \beta_e)J_e L r_{\bar{p}}}{e\beta_e c a_e^2 \gamma_{\bar{p}}}, \tag{21}$$

here $r_{\bar{p}} = 1.53 \cdot 10^{-18}$m is (anti)proton classical radius, relativistic antiproton factor $\gamma_{\bar{p}} \approx 1000$. E.g. with parameters of experiment $J_e = 1.5$A, $\beta_e = 0.2$, $L = 2.0$m, β_x=100m, $a_e = 1$mm, one gets $\Delta\nu_x = -0.0091$. Of course, there is no contribution in the coupling.

Now, let us write the electron density distortion in the form $\delta\rho(x, y) = xy \cdot C(x, y)$ which emphasize the product xy and the rest is a slowly varying function of xy:

$$C(x, y) = \frac{2eN_{\bar{p}}}{B}\frac{d\rho_0(r^2)}{d(r^2)} \cdot \frac{I(x, y)(\sigma_x^2 - \sigma_y^2)}{\sigma_x^2\sigma_y^2}. \tag{22}$$

The effective 2D skew potential can be found as a solution of following equation

$$\triangle V_{skew} = -4\pi\delta\rho\frac{r_{\bar{p}}}{\gamma_{\bar{p}}}, \tag{23}$$

that is approximately equal to:

$$V_{skew} \approx \frac{\pi r_{\bar{p}}}{6\gamma_{\bar{p}}} C(x,y)\cdot r^2 \cdot xy. \tag{24}$$

This yields corresponding coupling magnitude of

$$|\kappa| \approx \frac{\sqrt{\beta_x\beta_y} r_{\bar{p}}}{8\gamma_{\bar{p}}} < C(x,y)\cdot r^2 > . \tag{25}$$

Brackets $< ... >$ denote averaging over antiproton betatron oscillations. Now, one can estimate of the maximum coupling spread using Eqs.(16, 19-23) together with approximate relation $\beta_x \simeq 3\beta_y$

$$|\kappa| \approx |\Delta\nu_x| \frac{eN_{\bar{p}}}{2\sqrt{3}\sigma_x^2 B} \cdot < S(x,y) > \approx \frac{0.84[N_{\bar{p}}/6\cdot 10^{10}]}{\sigma_x^2[mm]B[kG]} \cdot < S(x,y) > . \tag{26}$$

Fig.7 shows numerical factor $S(x,y)$ for the two electron distributions satisfying Eq.(17) with $a_e = \sigma_x$ (left plot) and another with $a_e = 2.5\sigma_x$ (right plot). The maximum value of this factor of $S^{max}(x,y)$ =0.7 for slender electron beam and 0.13 for wider electron beam takes place at amplitudes of about electron beam size. The coupling vanishes for small betatron amplitude particles and at very large amplitudes. The effect is larger in the plane of the longer antiproton ellipse axis (horizontal in our case).

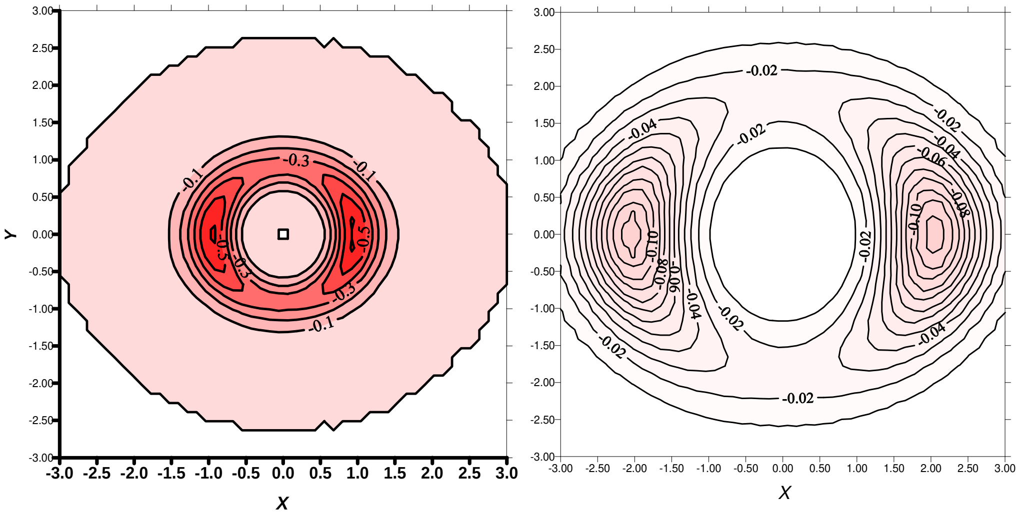

FIG. 7. Coupling functions $S(x,y)$ for antiproton betatron oscillations with thin (left) and wide electron beams (right).

Let us make numerical example with the same parameters we used above $\sigma_x = 0.61$mm, $N_{\bar{p}} = 6\cdot 10^{10}$, $\Delta\nu_x \simeq 0.01$. Maximum numerical factor is about $< S(x,y) >^{max} \approx 0.5 \cdot S^{max}(x,y)$, i.e. 0.35 for $a_e = 1\sigma_x$ and 0.065 for $a_e = 2.5\sigma_x$. Now, with solenoid field of $B = 2$T, one gets the maximum coupling spread $|\kappa| \simeq 4\cdot 10^{-4}$ for thin electron beam , and $7\cdot 10^{-5}$ for wider electron beam. Both of these values are rather small with respect to the Tevatron global coupling correction goal of about 0.001.

IV. CONCLUSIONS.

We have considered distortions of the electron beam in the beam-beam compensation set-up. It is found that rather low longitudinal field of about 1kG can help to avoid the beam blow up due to defocusing electron and antiproton space charge forces. Much higher solenoid field of about 2T is necessary to have electron charge distribution distortions within few percents with respect to original axisymmetric distribution. The need comes from a requirement to contribute much less $x-y$ coupling than other sources in the Tevatron collider ring and do not introduce significant spread of the coupling in the antiproton bunch. Both tracking with computer code $ZBEAM$ and analytical consideration have shown that the distortion is smaller if the electron beam size is several times the $\bar{p}$ beam size.

ACKNOWLEDGMENTS

We acknowledge stimulating and fruitful discussions with Vasily Parkhomchuk, Slava Danilov, Andrei Sery, Peter Bagley, and Alexei Burov.

One of us (A.Z.) thanks John Marriner and Dave Finley for invitation to visit FNAL and warm hospitality.

---

* Joint Institute for Nuclear Research, 141980 Dubna, Moscow region, Russia.

[1] V.Shiltsev, D.Finley, “Electron Compression” of Beam-Beam Tune Spread in the Tevatron”, FERMILAB-TM-2008 (1997).
[2] V.Shiltsev, “Electron Lens” to Compensate Bunch-To-Bunch Tune Spread in TEV33”, FERMILAB-TM-2031 (1997).
[3] J.P.Marriner, “The Fermilab Proton-Antiproton Collider Upgrades”, FERMILAB-Conf-96/391 (1996); S.D.Holmes, *et.al*, FNAL-TM-1920 (1995).
[4] V.Shiltsev, ed., “Contributions to the Mini-Workshop on Beam-Beam Compensation”, FERMILAB-Conf-98/064 (March 1998); V.Shiltsev, “Mini-Workshop on Beam-Beam Compensation in the Tevatron”, *Beam Dynamics Newsletter, No.16* (April 1998).
[5] E.Tsyganov and A.Zinchenko, “Charge Tracing Code for the SSC Environment”, SSCL-Preprint-618 (1993).
[6] J.E.Augustin, SLAC Note PEP-63 (1973);
B.W.Montague, CERN Report CERN/ISR-GS/75-36 (1975).
[7] P.Bagley and J.Annala, private communication.